Numerical Simulation of a Buoyant Methane/Air Diffusion Flame

D. MORVAN[1], B. PORTERIE[2] and J.C. LORAUD[2]
[1] IRPHE UMR CNRS 6594
[2] IUSTI UMR CNRS 6595
Technopôle de Château Gombert
13453 Marseille cedex 13 FRANCE

ABSTRACT

The unsteady behaviour of a buoyant methane diffusion flame is simulated numerically. The turbulent transport and the reactive mixture are evaluated using a $RNG - k - \epsilon - g$ turbulence modelling and a presumed shape (β-function) *pdf* approach. A fine description of radiation is achieved by using a two-equation submodels for the description of soot formation and a differential P1-approximation to calculate the irradiance field. The numerical results show that the buoyant flow above the flame is characterized by the development of large eddies on both sides of the column formed during the expansion of the hot gases. The growth of these buoyancy driven instabilities is also marked by an oscillatory behaviour as it can be noticed on the time evolution of the flame height.

INTRODUCTION

The control of phenomena occurring during the expansion of a fire requires the understanding of the physical mechanisms which govern the flame behaviour (combustion rate, flame temperature ...) and their interaction with the buoyant turbulent flow which develops in the vicinity of the flaming zone. Pool and natural fires are characterized by a very low initial momentum and are strongly affected by buoyancy effects [1]. To study the behaviour of this kind of fire, it is more convenient to perform experiments by injecting gaseous hydrocarbon through a porous burner, to obtain flow patterns in the combustion zone similar to those encountered for a fire and reproducible experimental conditions [2]. It is well known that the fire plume consists of three distinct regions: the persistent flame, the intermittent flame and the buoyant plume [3, 4]. Experimental studies have shown that oscillatory behaviour have been observed above buoyant diffusion flames [5, 6]. The formation of coherent structures above a fire plume results from the development of buoyancy driven instabilities, which, in turn, leads to vortex shedding and flame flickering. Most of numerical simulations based on statistical approach do not reproduced this unsteady behaviour [7] excepted more recent works developed from large eddy simulations (LES) [8] or RNG turbulence modelling [9]. Experimental investigations have shown relatively low centerline temperature levels, with a maximum value ranges from $1100K$ to $1300K$ representing approximately half of the flame temperature in adiabatic conditions. Two reasons can explain this divergence, the radiation heat transfer and the temperature fluctuations. Neglecting the radiation heat transfer, the flame temperatures predicted from statistical formulations remains higher than experimental data ($1600 - 2000K$). Including a radiation heat loss representing 50% of the energy released by the combustion reaction, the maximum temperature level can be reduced to $1300K$ [7, 1]. The modifications of the radiative properties of the gas mixture result from the formation of combustion products (CO, H_2O, CO_2) and soot particles in the flame. This last one represents in fact the most important contribution. It explains why the radiation heat loss for poor sooting gaseous fuels (such as methane) represents only $20 - 25\%$ of the chemical energy released

during the combustion. In most of proposed numerical studies, the radiation heat loss is introduced reducing the flame temperature or the energy released by the combustion [10]. The specificity of the present study is that the radiation heat transfer is not fixed a priori but is integrated in the calculation including the contributions due to combustion products and soot particles. Recent numerical results obtained from large eddy simulations [8] or RNG statistical turbulence modelling [9] have reproduced the pulsating behaviour which characterizes buoyant fires. These studies have also demonstrated that averaging the instantaneous temperatures allowed to find mean temperature distributions in agreement with experimental correlations obtained for a methane/air flame expanding from a square porous burner [11].
The configuration studied in the present paper is represented in Figure 1. A gaseous fuel (methane) is injected through a porous burner ($0.3m$ large); the dimensions of the 2D computational domain are $3m \times 3m$.

MATHEMATICAL FORMULATION

The variables transported (mass, momentum, energy ...) by the turbulent flow are decomposed as $\phi = \widetilde{\phi} + \phi''$ where $\widetilde{\phi}$ is defined as the average value of ϕ evaluated over a finite range of time Δt:

$$\widetilde{\phi} = \frac{1}{\Delta t}\int_{t}^{t+\Delta t} \phi(\tau)\, f\tau \tag{1}$$

Applying this averaging procedure to the instantaneous conservation equations of mass, momentum, energy ... and introducing a density-weighting formulation we obtain [12, 13, 5, 14]:

$$\frac{\partial \bar{\rho}}{\partial t} + \frac{\partial}{\partial x_j}\left(\bar{\rho}\widetilde{u_j}\right) = 0 \tag{2}$$

$$\frac{\partial}{\partial t}\left(\bar{\rho}\widetilde{u_i}\right) + \frac{\partial}{\partial x_j}\left(\bar{\rho}\widetilde{u_j}\widetilde{u_i}\right) = \frac{\partial \overline{\sigma_{ij}}}{\partial x_j} - \frac{\partial \overline{\rho u_j'' u_i''}}{\partial x_j} + \bar{\rho} g_i \tag{3}$$

$$\frac{\partial}{\partial t}\left(\bar{\rho}\widetilde{h}\right) + \frac{\partial}{\partial x_j}\left(\bar{\rho}\widetilde{u_j}\widetilde{h}\right) = \frac{\partial}{\partial x_j}\left(\frac{\bar{\mu}}{Pr}\frac{\partial \widetilde{h}}{\partial x_j}\right) + \frac{\partial \bar{p}}{\partial t} - \frac{\partial \overline{\rho u_j'' h''}}{\partial x_j} - \frac{\partial \overline{q_j^R}}{\partial x_j} \tag{4}$$

where $\overline{\sigma_{ij}}$ is the average stress tensor expressed as

$$\overline{\sigma_{ij}} = -\bar{p} + \bar{\mu}\left(\frac{\partial \widetilde{u_i}}{\partial x_j} + \frac{\partial \widetilde{u_j}}{\partial x_i} - \frac{2}{3}\frac{\partial \widetilde{u_k}}{\partial x_k}\delta_{ij}\right) \tag{5}$$

where u_i, h, g_i, q_j^R, ρ, μ are the velocity components, the enthalpy, the gravity acceleration, the radiative heat flux, the density, and the viscosity, respectively. The superscripts ($\bar{}$), ($\widetilde{}$), and ($''$) denote time average, density-weighted Favre average and density-weighted Favre fluctuation. In fact this procedure is comparable to Large Eddy Simulations (LES), in the present case the equations are transformed using a time filtering. This method allows to follow the formation and the dynamics of coherent structures which are present in the plume and which contribute significantly to the interaction between the flame and the near field region. The contribution due to the small scale structures is represented using the Boussinesq's eddy viscosity concept:

$$-\overline{\rho u_j'' u_i''} = \mu_t\left(\frac{\partial \widetilde{u_i}}{\partial x_j} + \frac{\partial \widetilde{u_j}}{\partial x_i}\right) - \frac{2}{3}\left(\mu_t\frac{\partial \widetilde{u_k}}{\partial x_k} + \bar{\rho}k\right)\delta_{ij} \tag{6}$$

$$\mu_t = \bar{\rho} C_\mu \frac{k^2}{\epsilon} \tag{7}$$

To calculate the corresponding turbulent contributions in the scalar transport equations, a gradient diffusion model is used:

$$-\overline{\rho u_j'' \phi''} = \frac{\mu_t}{\sigma_\phi}\frac{\partial \widetilde{\phi}}{\partial x_j} \tag{8}$$

δ_{ij} is the Kronecker delta and σ_ϕ the turbulent Prandtl/Schmidt number for ϕ.
where k and ϵ are, respectively, the turbulence kinetic energy and its dissipation rate.
To avoid the unphysical behaviour obtained with standard $k-\epsilon$ turbulence modelling for the calculation of weak turbulent flows [15], a set of modified transport equations for k and ϵ derived from the Renormalization Group (RNG) theory [16, 17] is used:

$$\frac{\partial}{\partial t}(\bar{\rho}k)+\frac{\partial}{\partial x_j}(\bar{\rho}\tilde{u_j}k)=\frac{\partial}{\partial x_j}\left[\left(\overline{\mu}+\frac{\mu_t}{\sigma_k}\right)\frac{\partial k}{\partial x_j}\right]+P_k+W_k-\bar{\rho}\epsilon \tag{9}$$

$$\frac{\partial}{\partial t}(\bar{\rho}\epsilon)+\frac{\partial}{\partial x_j}(\bar{\rho}\tilde{u_j}\epsilon)=\frac{\partial}{\partial x_j}\left[\left(\overline{\mu}+\frac{\mu_t}{\sigma_\epsilon}\right)\frac{\partial \epsilon}{\partial x_j}\right]+(C_{\epsilon 1}-R)\frac{\epsilon}{k}P_k+C_{\epsilon 3}\frac{\epsilon}{k}W_k-C_{\epsilon 2}\bar{\rho}\frac{\epsilon^2}{k} \tag{10}$$

where P_k and W_k are respectively the shear and buoyancy turbulent production terms:

$$P_k=-\overline{\rho u_i'' u_j''}\frac{\partial \tilde{u}_i}{\partial x_j} \quad W_k=-\frac{\mu_t}{\bar{\rho}^2}\frac{\partial \bar{\rho}}{\partial x_j}\frac{\partial \bar{p}}{\partial x_j} \quad R=\frac{\eta(1-\eta/\eta_0)}{1+\beta\eta^3} \tag{11}$$

$$\eta=\sqrt{\frac{P_k}{C_\mu \bar{\rho}\epsilon}} \quad \eta_0=4.38 \quad \beta=0.015 \quad C_\mu=0.0845 \tag{12}$$

$$C_{\epsilon 1}=1.42 \quad C_{\epsilon 2}=1.68 \quad C_{\epsilon 3}=1.5 \quad \sigma_k=0.7179 \quad \sigma_\epsilon=1.3 \tag{13}$$

The turbulent reacting gas mixture is evaluated using presumed pdf-β-function method:

$$\widetilde{P_\beta}(f)=\frac{f^{a-1}(1-f)^{b-1}}{\int_0^1 f^{a-1}(1-f)^{b-1}} \tag{14}$$

$$\text{with } a=\tilde{f}\gamma, \quad b=\left(1-\tilde{f}\right)\gamma \quad \text{and } \gamma=\frac{\tilde{f}\left(1-\tilde{f}\right)-\tilde{g}}{\tilde{g}} \tag{15}$$

where a and b can be determined from the values of mean mixture fraction ($\tilde{f}$) and its variance ($\tilde{g}=\widetilde{f''^2}$), solutions of the following transport equations [13, 10]

$$\frac{\partial}{\partial t}\left(\bar{\rho}\tilde{f}\right)+\frac{\partial}{\partial x_j}\left(\bar{\rho}\tilde{u_j}\tilde{f}\right)=\frac{\partial}{\partial x_j}\left[\left(\frac{\bar{\mu}}{Pr}+\frac{\bar{\mu}_t}{\sigma_f}\right)\frac{\partial \tilde{f}}{\partial x_j}\right] \tag{16}$$

$$\frac{\partial}{\partial t}(\bar{\rho}\tilde{g})+\frac{\partial}{\partial x_j}(\bar{\rho}\tilde{u_j}\tilde{g})=\frac{\partial}{\partial x_j}\left[\left(\frac{\bar{\mu}}{Pr}+\frac{\bar{\mu}_t}{\sigma_g}\right)\frac{\partial \tilde{g}}{\partial x_j}\right]+C_{g_1}\mu_t\left(\frac{\partial \tilde{g}}{\partial x_j}\right)^2-C_{g_2}\bar{\rho}\frac{\epsilon}{k}\tilde{g} \tag{17}$$

(with $C_{g_1}=2.8$, $C_{g_2}=2.0$ and $\sigma_g=\sigma_f=0.7$)

The Favre-averaged mass fraction of species i is then determined from

$$\tilde{Y}_i=\int_0^1 Y_i(f)\widetilde{P_\beta}(f)df \tag{18}$$

For the present study, a one-step irreversible reaction (methane/air) is used, assuming that $Y_i(f)$ are linear functions except at the stoichiometric value f_{st} [10]. The enthalpy-temperature dependence is treated using CHEMKIN thermodynamic data base [18].
Various experimental measurements have shown that radiative heat transfer cannot be neglected for a good evaluation of the energy balance in a laminar or a turbulent diffusion flame. The radiative heat loss can represent $20-50\%$ of the chemical energy released during the combustion reaction [14, 1]. Two mechanisms contribute to radiative heat loss, namely the radiation of the combustion products (CO_2 and H_2O) and the radiation of soot particles in the flame [19, 20, 14]. If soots are represented by spherical pure carbon particles, two variables are necessary to represent the soot field, respectively the number density n_s and the volume fraction f_v:

$$\frac{\partial}{\partial t}(\bar{\rho}\widetilde{n_s})+\frac{\partial}{\partial x_j}(\bar{\rho}\tilde{u_j}\widetilde{n_s})=-\frac{\partial}{\partial x_j}\left(\bar{\rho}\widetilde{u_j^{th}n_s}\right)+\frac{\partial}{\partial x_j}\left(\frac{\bar{\mu}_t}{\sigma_f}\frac{\partial \widetilde{n_s}}{\partial x_j}\right)+\overline{\rho\dot{\omega}_{n_s}} \tag{19}$$

$$\frac{\partial}{\partial t}\left(\bar{\rho}\tilde{f}_v\right)+\frac{\partial}{\partial x_j}\left(\bar{\rho}\tilde{u}_j\tilde{f}_v\right)=-\frac{\partial}{\partial x_j}\left(\bar{\rho}\widetilde{u_j^{th}f_v}\right)+\frac{\partial}{\partial x_j}\left(\frac{\bar{\mu}_t}{\sigma_f}\frac{\partial \tilde{f}_v}{\partial x_j}\right)+\overline{\rho\dot{\omega}_{f_v}} \tag{20}$$

where the source terms representing the different contributions to the soot production phenomena (nucleation, coagulation, oxidation, surface growth) are evaluated as

$$\overline{\rho\dot{\omega}_{n_s}} = \underbrace{N_0 C_\alpha \bar{\rho}^3 \widetilde{T}^{1/2} \widetilde{X_{Fu}} e^{-T_\alpha/\widetilde{T}}}_{nucleation} - \underbrace{\bar{\rho} C_\beta \widetilde{T}^{1/2} \frac{\widetilde{n_s}^2}{N_0}}_{coagulation} - \underbrace{\frac{(36\pi)^{1/3} W_{Ox} \widetilde{n_s}^{4/3}}{\rho_{soot} \widetilde{f_v}^{1/3}}}_{oxidation} \tag{21}$$

$$\overline{\rho\dot{\omega}_{f_v}} = \underbrace{\frac{C_\delta C_\alpha}{\rho_{soot}} \bar{\rho}^3 \widetilde{T}^{1/2} \widetilde{X_{Fu}} e^{-T_\alpha/\widetilde{T}}}_{nucleation} + \underbrace{\frac{C_\gamma}{\rho_{soot}^{1/3}} \widetilde{n_s}^{1/3} \widetilde{f_v}^{2/3} \bar{\rho}^2 \widetilde{T}^{1/2} \widetilde{X_{Fu}} e^{-T_\gamma/\widetilde{T}}}_{surface\ growth}$$

$$- \underbrace{\frac{(36\pi)^{1/3} W_{Ox} \widetilde{n_s}^{1/3} \widetilde{f_v}^{2/3}}{\rho_{soot}}}_{oxidation} \tag{22}$$

u_j^{th} is the mean thermophoretic velocity component in the j-direction:

$$\widetilde{u_j^{th}} = -0.54\nu \frac{\partial \ln \widetilde{T}}{\partial x_j} \tag{23}$$

ρ_{soot} is the soot particle density ($1.8 g/cm^3$), C_α, C_β, C_δ, C_γ, T_α, T_γ the coefficients and activation temperatures

$$C_\alpha = 6.54 \times 10^4 cm^3/g^2 \cdot K^{1/2} \cdot s,$$
$$C_\beta = 1.3 \times 10^{13} cm^3/K^{1/2} \cdot s,$$
$$C_\delta = 1.44 \times 10^5 g,$$
$$C_\gamma = 1.0 \times 10^3 cm^3/g^{2/3} \cdot K^{1/2} \cdot s,$$
$$T_\alpha = 4.61 \times 10^4 K,$$
$$T_\gamma = 1.26 \times 10^4 K,$$
$$N_0 = 6.02214 \times 10^{23} mol^{-1} \text{ Avogadro's number}).$$

The term W_{Ox} relative to soot oxidation on the right-hand side of eqs (21) and (22) corresponds to soot oxidation, it is evaluated from the rate for oxidation of pyrolytic graphite [21],

$$W_{Ox} = 120 \left[\frac{k_A P_{O_2}}{1 + k_z P_{O_2}} \chi + P_{O_2} (1 - \chi) \right] \tag{24}$$

$$\chi = \frac{1}{1 + \frac{k_T}{k_B P_{O_2}}} \tag{25}$$

where P_{O_2} is the partial pressure of oxygen

$$k_A = 20 \exp\left(-30000/R\widetilde{T}\right) g/cm^2.s.atm \tag{26}$$

$$k_B = 4.46 \quad 10^{-3} \exp\left(-15200/R\widetilde{T}\right) g/cm^2.s.atm \tag{27}$$

$$k_T = 1.51 \quad 10^5 \exp\left(-97000/R\widetilde{T}\right) g/cm^2.s \tag{28}$$

$$k_z = 21.3 \exp\left(4100/R\widetilde{T}\right) atm^{-1} \tag{29}$$

For the radiation heat transfer, the gas-soot mixture can be considered as a gray medium characterized by an absorption coefficient including the contributions of combustion products and soot particles. Then the irradiance field and the radiative heat flux can be calculated by solving the Radiative Transfer Equation (RTE) developed using the P1-approximation [22, 23]:

$$\frac{\partial}{\partial x_j} \left(\frac{1}{3a_R} \frac{\partial J}{\partial x_j} \right) = a_P \left[J - 4n^2 \sigma \widetilde{T}^4 \right] \tag{30}$$

$$-\frac{\partial \overline{q_j^R}}{\partial x_j} = a_P \left[J - 4n^2 \sigma \widetilde{T}^4 \right] \tag{31}$$

For methane/air flame the absorption coefficient can be approximated as [19]:

$$a_R = a_P = a_{Pro} + a_{soot} = 0.1\widetilde{X_{Pro}} + 1862\widetilde{f_v}\widetilde{T} \quad (m^{-1}) \tag{32}$$

To obtain an accurate representation of such turbulent reactive flow, including unsteady behaviour and high gradient regions (shear layer, combustion front), the set of partial differential equations previously described is solved using a Finite Volume method including a second order backward Euler scheme for the time integration and an Ultra-Sharp method for the evaluation of convection-diffusion fluxes between two adjacent control volumes [24]. This method combines the use of a high order upwind convective scheme introducing no numerical diffusion, with a flux limiter strategy which damp the oscillations sometimes introduced by this kind of scheme. The pressure-velocity coupling is treated using a non iterative algorithm based on a projection method [13]. At the open boundaries zero shear stress is assumed and the normal velocity component is evaluated from continuity equation using a pressure correction procedure. For the other variables ($\widetilde{T}, k, \epsilon, \widetilde{Y_i}$ ...) a zero flux condition is assumed for outlet flow and far field conditions ($\widetilde{T} = 300K, k = \epsilon = 10^{-6}, \widetilde{Y_i} = \widetilde{Y_i^0}$ ...) for inlet flow.

NUMERICAL RESULTS AND DISCUSSION

The results reported in the present paper have been performed for a 140 × 70 cartesian grid. To obtain an accurate representation of the boundary layer flow along the bottom boundary and the region where the chemical reaction occurs, the mesh is locally refined near the lower boundary and on both sides of the burner axis. The calculations are performed on PC (Intel Pentium Pro 200Mz), 60s of flame simulation takes approximatively 4-6 hours of CPU time (using an average time steps $\Delta t = 10^{-2}$). The inlet fuel velocity has been adjusted to obtain a $150kW/m$ pool fire. The instantaneous temperature field reported in Figure 2, exhibits a dissymmetrical pattern. The maximum temperature is relatively high ($T \approx 2000K$) (to compare with the instantaneous adiabatic flame temperature for methane is $T = 2250K$). The stoichiometric flame contour is represented in Figure 4. As previously mentioned for the temperature field, the development of coherent structures on both sides of the fire induces a flickering of the flame surface. This instability is also observed on the time evolution of the flame height reported in Figure 5. The frequency associated to the unsteady behaviour is about $0.7Hz$ (see Figure 5) which indicates that probably only a part of the unsteady motion is represented in the present calculation (for the same Froude number $Fr \approx 10^{-4}$ experimental correlations indicate a vortex shedding frequency $f \approx 2.7Hz$ [6, 25]). The present simulation can be interpreted as a temporal filtering [26] and therefore all the flow structures (and their corresponding consequences upon the flame dynamics) cannot be represented. The present study is limited to 2D calculations as the physical problem is 3D which can also explain this divergence. The volume fraction of soot is represented in Figure 3, with a maximum value observed in the flame $||f_v||_\infty \approx 2.2\ 10^{-7}$ which is in agreement with experimental values measured for methane/air diffusion flame [19]. Figure 6 shows the instantaneous and time averaged (over $10s$) centerline temperature compared to experimental correlation [11] extended to a line fire configuration assuming that for a rectangular burner beyond a length/width shape ratio equal to 3 the centerline temperature depends only on fire power density (kW/m). As already mentioned in the literature [8] the curve representing the instantaneous temperature is characterized by large amplitude oscillations due to the flickering of the flame surface. In this case the maximum in temperature is about $1900K$ which is in agreement with the experimental values measured for steady methane/air flame [19]. The time averaged centerline temperature curve exhibits a more regular behaviour with a maximum in temperature reduced to $\approx 1500K$ which is in agreement with the numerical results obtained from large eddy simulations [8]. Above the flame in the buoyant plume, the decreasing rate of the centerline temperature is similar to experimental correlations [11]. In Figures 7 and 8 the centerline soot volume fraction and mean soot diameter are represented. These two curves indicate that soot oxidation is complete as the temperature exceeds $1600K$. The maximum soot particle radius is about $70nm$ which is in accordance with the value observed for a methane/air diffusion flame [19].

References

[1] P. Joulain, "Convective and radiative transport in pool and wall fires: 20 years of research in poitiers", in Fire Safety Journal, 26:99–149, 1996.

[2] B.J. McCaffrey, "Purely buoyant diffusion flames: some experimental results", Technical report, National Bureau of Standards, 1979.

[3] D. Drysdale, An introduction to fire dynamics, John Wiley and sons, 1985.

[4] G. Cox, Combustion fundamentals of fire, Academic Press, 1995.

[5] G. Cox. "Basic considerations", in Combustion fundamentals of fire, pages 1–30. Academic Press, G. Cox (Editor), 1995.

[6] M.A. Delichatsios, "Gravitational fluctuations in pool fires and pool buoyant flows", in Combust. Sci. and Technol., 112:355–358, 1996.

[7] M. Annarumma, J.M. Most, and P. Joulain, "On the numerical modeling of buoyancy-dominated turbulent vertical diffusion flames", in Combust. Flame, 85:403–415, 1991.

[8] K.B. McGrattan, H.R. Baum, and R.G. Rehm, "Large eddy simulations of smoke movement", in Fire Safety Journal, 30:162–178, 1998.

[9] D. Morvan, B. Porterie, M. Larini, and J.C. Loraud, "Numerical simulation of methane/air turbulent pool fire", in Proceedings 1st Int. Symposium on Advances in Computational Heat Transfer, pages 184–191, 26-30 May 1997. Çeşme, Turkey.

[10] J. Hernandez, A. Crespo, and N.J. Duijm, "Numerical modelling of turbulent jet diffusion flames in the atmospheric surface layer", in Combust. Flame, 101:113–131, 1995.

[11] H.R. Baum and B.J. McCaffrey, "Fire induced flow field-theory and experiment", in Fire Safety Science Proceedings 2nd Int. Symp., pages 129–148, 1989.

[12] R. Borghi, "Turbulent combustion modelling", Prog. Energy Combust. Sci., 14:245–292, 1988.

[13] P.A. Libby and F.A. Williams, Turbulent Reacting Flows. Academic Press, 1993.

[14] J.B. Moss, "Turbulent diffusion flames", in Combustion fundamentals of fire, pages 221–272. Academic Press, G. Cox (Editor), 1995.

[15] C.G. Speziale, Modeling of turbulent transport equations, pages 185–242. Oxford University Press, 1996.

[16] V. Yakhot and S.A. Orszag, "Renormalization group analysis of turbulence", in J. Scientific Computing, 1(1):3–51, 1986.

[17] V. Yakhot and M. Smith, "The renormalization group, the ϵ-expension and derivation of turbulence models", in J. Scientific Computing, 7(1):35–61, 1992.

[18] R.J. Kee, F.M. Rupley, and J.A. Miller, The chemkin thermodynamic data base, Technical report, Sandia National Laboratories, 1992.

[19] C.R. Kaplan, C.R. Shaddix, and K.C. Smyth, "Computations of enhanced soot production in time-varying ch_4/air diffusion flames", in Combust. Flame, 106:392–405, 1996.

[20] K.J. Syed, C.D. Stewart, and J.B. Moss, "Modelling soot formation and thermal radiation in buoyant turbulent diffusion flames", in 23rd Symposium. (International) on Combustion, The combustion Institute, page 1533, 1990.

[21] J. Nagle and R.F. Strickland-Constable, "Oxidation of carbon between $1000-2000^o c$", in Proceedings 5th Conference on Carbon, volume 1, pages 154–164, 1962.

[22] T. Fusegi and B. Farouk, "Laminar and turbulent natural convection-radiation interactions in a square enclosure filled with a nongray gas", in Numerical Heat Transfer, Part A, 15:303–322, 1989.

[23] G. Lauriat, "Combined radiation-convection in gray fluids enclosed in vertical cavities", in J. Heat Transfer, 104:609-615, 1982.

[24] B.P. Leonard and S. Mokhtari, "Beyond first-order upwinding: the ultra-sharp alternative for non-oscillatory steady-state simulation of convection", in Int. J. Numerical Methods Engineering, 30:729-766, 1990.

[25] P. Joulain, "The behavior of pool fires: state of the art and new insights", in 27th Symposium. (International) on Combustion, The combustion Institute, 1998.

[26] G. Billet, "Simulation des écoulements transitionnels turbulents non-réactifs et réactifs à grand nombre de reynolds par une méthode l.e.s. à filtrage temporel", Technical report, ONERA, 1996.

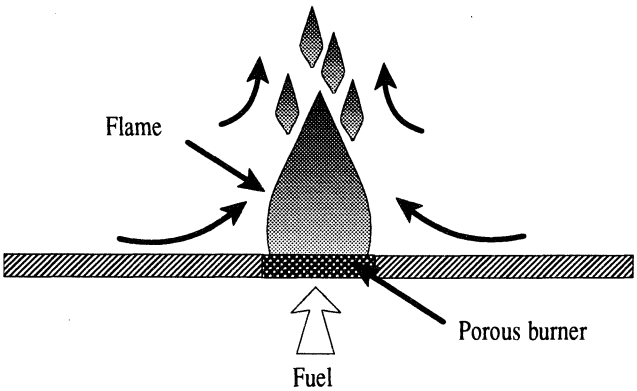

Figure 1: Buoyant turbulent diffusion flame expanding from a porous burner.

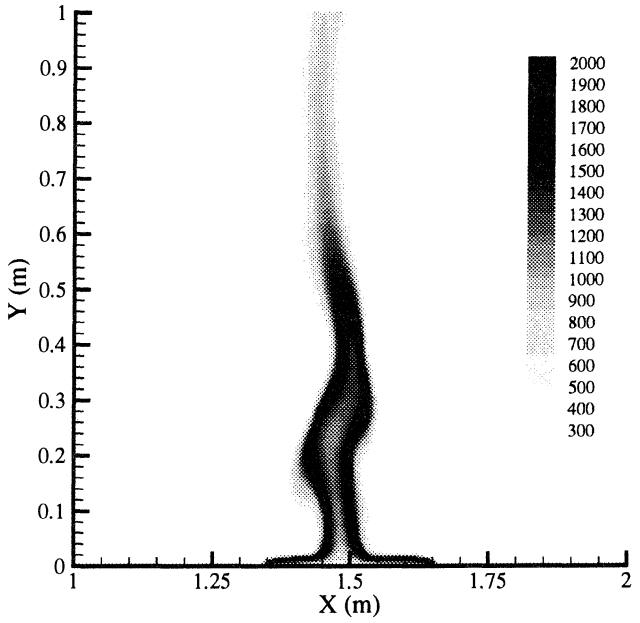

Figure 2: Closer view of the computed temperature field of a $150kW/m$ buoyant turbulent diffusion flame using a 140×70 grid.

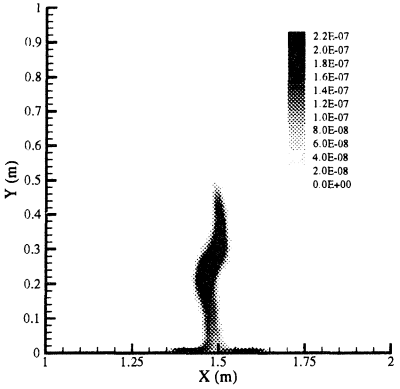

Figure 3: Closer view of the computed of soot volume fraction field of a $150kW/m$ buoyant turbulent diffusion flame.

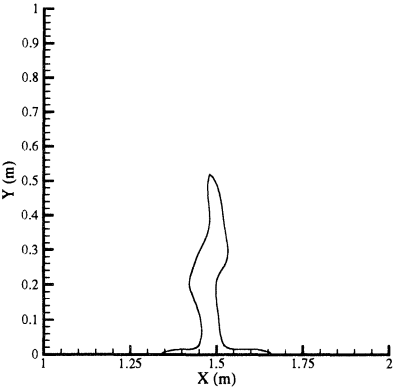

Figure 4: Stoichiometric contour of a $150kW/m$ buoyant turbulent diffusion flame.

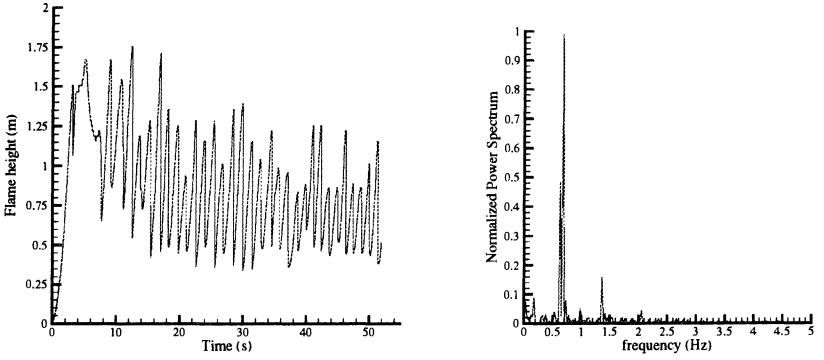

Figure 5: Time evolution and normalized power spectrum of the stoichiometric flame height of a $150kW/m$ buoyant turbulent diffusion flame.

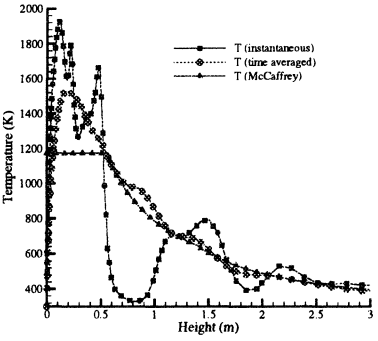

Figure 6: A comparison of the centerline temperature (instantaneous and time averaged) of a $150kW/m$ buoyant turbulent diffusion flame with that deduced from the correlation of McCaffrey [11].

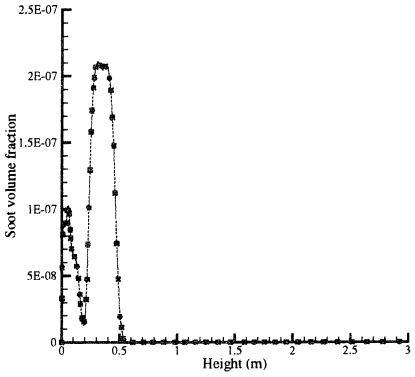

Figure 7: Centerline soot volume fraction of a $150kW/m$ buoyant turbulent diffusion flame.

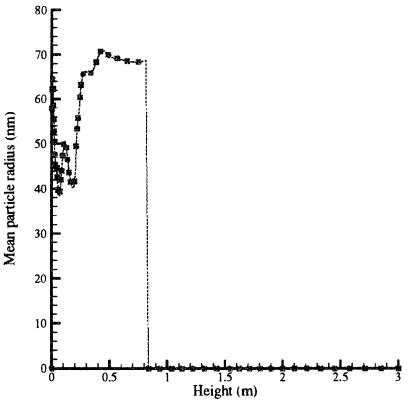

Figure 8: Centerline mean soot particle diameter of a $150kW/m$ buoyant turbulent diffusion flame